

# Fast Beam Training and Alignment for IRS-Assisted Millimeter Wave/Terahertz Systems

Peilan Wang, Jun Fang, Wei Zhang *Fellow, IEEE* and Hongbin Li, *Fellow, IEEE*

**Abstract**—Intelligent reflecting surface (IRS) has emerged as a competitive solution to address blockage issues in millimeter wave (mmWave) and Terahertz (THz) communications due to its capability of reshaping wireless transmission environments. Nevertheless, obtaining the channel state information of IRS-assisted systems is quite challenging because of the passive characteristics of the IRS. In this paper, we develop an efficient downlink beam training/alignment method for IRS-assisted mmWave/THz systems. Specifically, by exploiting the inherent sparse structure of the base station-IRS-user cascade channel, the beam training problem is formulated as a joint sparse sensing and phaseless estimation problem, which involves devising a sparse sensing matrix and developing an efficient estimation algorithm to identify the best beam alignment from compressive phaseless measurements. Theoretical analysis reveals that the proposed method can identify the best alignment with only a modest amount of training overhead. Numerical results show that, for both line-of-sight (LOS) and NLOS scenarios, the proposed method obtains a significant performance improvement over existing state-of-the-art methods. Notably, it can achieve performance close to that of the exhaustive beam search scheme, while reducing the training overhead by 95%.

**Index Terms**—Intelligent reflecting surface, millimeter wave communications, beam training/alignment.

## I. INTRODUCTION

Intelligent reflecting surface (IRS) has emerged as a competitive solution to address blockage issues and extend the coverage in millimeter wave (mmWave) and Terahertz (THz) communications [1]–[4]. To reap the gain brought by the large number of passive elements, instantaneous channel state information (CSI) is required for joint active and passive beamforming for IRS-assisted systems [5]–[12]. Nevertheless, CSI acquisition is challenging for IRS-assisted mmWave/THz systems due to the passive characteristics of the IRS and the large size of the channel matrix. Recently, some studies proposed to utilize the inherent sparse/low-rank structure of

the cascade base station (BS)-IRS-user mmWave channel, and cast channel estimation into a compressed sensing framework [13]–[16]. The proposed methods, however, suffer several drawbacks. Firstly, sparse/low-rank signal recovery via optimization methods or other heuristic methods usually incurs a high computational complexity which might be excessive for practical systems. Secondly, compressed sensing methods require accurate phase information of the received measurements. While in mmWave bands, the carrier frequency offset (CFO) effect and the random phase noise are more significant than that in sub-6GHz bands [17]–[19]. As a result, the phase of the measurements might be corrupted and unavailable for channel estimation. In [20], an aggregated channel estimation approach was proposed for IRS-assisted cell-free massive MIMO systems, where the reflecting coefficients of the IRS are pre-configured and thus only the equivalent channel between the access point and the user (also referred to as aggregated channel) needs to be estimated. The aggregated channel can then be estimated via traditional channel estimation methods. Nevertheless, this approach needs to pre-configure IRS's reflecting coefficients based on statistical CSI, thus may suffer a beamforming gain loss as compared with those beamforming approaches that are based on instantaneous CSI.

To address the above difficulties, instead of obtaining the full CSI, we focus on the problem of beam training whose objective is to acquire the angle of departure (AoD) and the angle of arrival (AoA) associated with the dominant path between the BS and the user. Beam training/alignment is an important topic that has been extensively investigated in conventional mmWave systems, e.g. [18], [21]–[26]. Nevertheless, beam alignment for IRS-assisted systems is more challenging as we need to simultaneously align the BS-IRS link as well as the IRS-user link. So far there are only a few attempts made on beam alignment for IRS-assisted mmWave systems, e.g. [27]–[30]. Specifically, [27] proposed a hierarchical beam search scheme for IRS-assisted THz systems. The proposed scheme, however, requires the BS to interact with each user individually, which may not be feasible at the initial channel acquisition stage. In [28], a multi-beam sweeping method based on grouping-and-extracting was proposed for beam training for IRS-assisted mmWave systems. This work assumes that the BS has aligned its beam to the LOS component between the BS and the IRS, and then focuses on the beam training between the IRS and the user. Nevertheless, in practice, the location information of the IRS may not be available to the BS, in which case one needs to perform a joint BS-IRS-user beam training. Recently, [29] proposed a random beamforming-based maximum likelihood

Peilan Wang, and Jun Fang are with the National Key Laboratory of Science and Technology on Communications, University of Electronic Science and Technology of China, Chengdu 611731, China, Email: peilan\_wangle@std.uestc.edu.cn, JunFang@uestc.edu.cn

Wei Zhang is with the School of Electrical Engineering and Telecommunications, The University of New South Wales, Sydney, Australia, E-mail: wzhang@ee.unsw.edu.au

Hongbin Li is with the Department of Electrical and Computer Engineering, Stevens Institute of Technology, Hoboken, NJ 07030, USA, E-mail: Hongbin.Li@stevens.edu

This work was supported in part by the National Science Foundation of China under Grant 61829103.

©2021 IEEE. Personal use of this material is permitted. Permission from IEEE must be obtained for all other uses, in any current or future media, including reprinting/republishing this material for advertising or promotional purposes, creating new collective works, for resale or redistribution to servers or lists, or reuse of any copyrighted component of this work in other works.

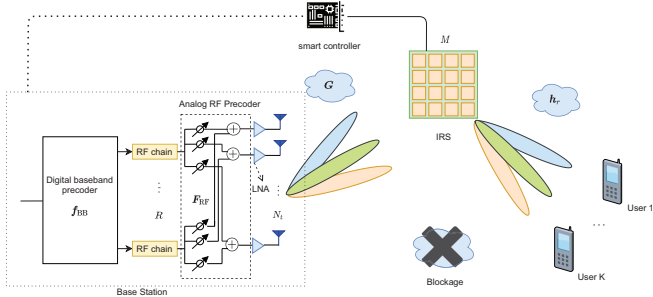


Fig. 1. IRS-assisted mmWave downlink multi-user systems.

(ML) estimation method to estimate the parameters associated with the LOS component, by treating other NLOS components as interference. In [30], an uplink beam training scheme was proposed for IRS-based multi-antenna multicast systems, where the IRS is used as a component of the transmitter.

In this paper, we propose an efficient beam training scheme for IRS-assisted mmWave/THz downlink systems. The key idea of our proposed method is to let both the transmitter and the IRS form multiple narrow beams to scan the angular space. Specifically, the proposed beam training process consists of a few rounds of “full-coverage scanning”, where in each full-coverage scanning, the entire space is efficiently scanned using pre-designed multi-directional beam training sequences. Also, in different rounds of full-coverage scanning, we use different combinations of directions to scan the angular space. Such a diversity allows us to identify the best beam alignment via an efficient set-intersection-based scheme. Theoretical analysis suggests that the proposed method can identify the best alignment with only a modest amount of training overhead.

It should be noted that although both the current work and [31] employ multi-directional beam sequences for downlink training, there are some major distinctions between these two works. Specifically, the work [31] considered downlink training in OFDM systems, where a same directional beam can be scaled by different factors at different subcarriers. This feature was utilized such that different directional beams can be distinguished from each other, and thus the CSI can be conveniently extracted. Nevertheless, such a scheme fails when single-carrier systems are considered because the modulation vector degenerates into a scalar which is no longer an effective fingerprint to distinguish different directional beams. In contrast, our proposed method does not rely on any modulation vector to identify the correct beam and works for single-carrier systems.

The rest of the paper is organized as follows. In Section II, the system model and the problem formulation are discussed. In Section III, we study how to devise the active and passive beam training sequences. In Section IV and Section V, we develop efficient set-intersection-based methods for LOS and NLOS scenarios to identify the best alignment based on compressive phaseless measurements. Simulation results are provided in Section VI, followed by concluding remarks in Section VII.

## II. SYSTEM MODEL AND PROBLEM FORMULATION

### A. Downlink Training and System Model

We consider the problem of downlink training and beam alignment in an IRS-assisted mmWave/THz multi-user system, where an IRS is deployed to assist the data transmission from the BS to a number of single-antenna users (see Fig. 1).

Before proceeding, we first provide a discussion of our proposed downlink training protocol. In the downlink beam training stage, the BS periodically broadcasts a pre-designed common beam training sequence  $\{\mathbf{f}(t)\}_{t=1}^T$ , and at the same time the IRS uses a common reflection beam sequence  $\{\mathbf{v}(t)\}_{t=1}^T$  to reflect the signal coming from the BS. For simplicity, we assume that the direct link from the BS to each user is blocked due to unfavorable conditions, and the transmitted signal arrives at each user via the reflected BS-IRS-user channel<sup>1</sup>. Each user receives signals reflected from the IRS, and estimates the angular parameters associated with the dominant path of its own downlink channel. This information is then sent by this user to the BS via a dedicated channel. A connection can thus be established between the BS and each user after the BS receives the related channel information associated with this user. The schematic of the downlink training protocol is also illustrated in Fig. 2.

In this downlink training framework, we are interested in studying *how to jointly devise the active/passive beam training sequences and estimate the channel parameters* to achieve fast beam alignment between the BS and each user. Note that since channel estimation is performed at each user and the design of beam training sequences is independent of users, our study can be simplified to single-user scenarios. Therefore in the rest of the paper, we consider the scenario where there is only a single user in the system. Also, in our setup, we assume that the BS has no knowledge of the geographical location of all facilities, including the IRS, the user and the BS itself.

To more rigorously formulate our problem, we now proceed to discuss our system model. The BS is equipped with  $N_t$  antennas and  $R \ll N_t$  radio frequency (RF) chains. At the BS, a digital baseband precoder  $\mathbf{f}_{\text{BB}} \in \mathbb{C}^R$  is first applied to a broadcast signal  $s$ , then followed by an analog RF beamformer  $\mathbf{F}_{\text{RF}} \in \mathbb{C}^{N_t \times R}$ . The transmitted training signal at the  $t$ th time instant can be written as

$$\mathbf{x}(t) = \mathbf{F}_{\text{RF}}(t)\mathbf{f}_{\text{BB}}(t)s(t) = \mathbf{f}(t)s(t), \quad (1)$$

where  $\mathbf{f}(t) \triangleq \mathbf{F}_{\text{RF}}(t)\mathbf{f}_{\text{BB}}(t)$  is the transmitter’s beamforming vector, and we set  $s(t) = 1$  in the beam training stage. Let  $\mathbf{G} \in \mathbb{C}^{M \times N_t}$  denote the channel from the BS to the IRS, and  $\mathbf{h}_r \in \mathbb{C}^M$  denote the channel from the IRS to the user. The IRS is a planar array consisting of  $M = M_y \times M_z$  passive reflecting elements. Each reflecting element of the IRS can reflect the incident signal with a reconfigurable phase shift and amplitude via a smart controller. Let  $\phi_m(t) \in [0, 2\pi]$  and  $\zeta_m(t) \in [0, 1]$  denote the phase shift and amplitude coefficients

<sup>1</sup>When the direct link between the BS and the user is available, we can first switch off the IRS and perform downlink training of the direct link using conventional mmWave beam training schemes. The effect of the direct link can then be canceled when we perform downlink BS-IRS-user training.

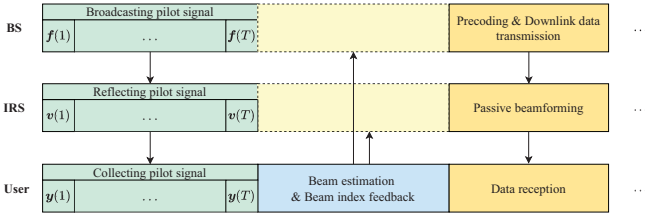


Fig. 2. Frame structure for the proposed joint BS-IRS-user beam training protocol.

adopted by the  $m$ th element at the  $t$ th time instant. Define

$$\Phi(t) \triangleq \text{diag}(\zeta_1(t)e^{j\phi_1(t)}, \dots, \zeta_M(t)e^{j\phi_M(t)}) \in \mathbb{C}^{M \times M}. \quad (2)$$

as the IRS reflecting matrix. The training signal received by the user can thus be expressed as

$$\begin{aligned} z(t) &= \mathbf{h}_r^H \Phi(t) \mathbf{G} \mathbf{x}(t) + n(t) \\ &= \mathbf{v}^H(t) \text{diag}(\mathbf{h}_r^H) \mathbf{G} \mathbf{f}(t) + n(t) \\ &= \mathbf{v}^H(t) \mathbf{H} \mathbf{f}(t) + n(t) \end{aligned} \quad (3)$$

where  $\mathbf{v}(t) \triangleq [\zeta_1(t)e^{j\phi_1(t)} \dots \zeta_M(t)e^{j\phi_M(t)}]^H$  is the passive reflecting vector,  $\mathbf{H} \triangleq \text{diag}(\mathbf{h}_r^H) \mathbf{G} \in \mathbb{C}^{M \times N_t}$  is referred to as the cascade channel, and  $n(t) \sim \mathcal{CN}(0, \sigma^2)$  represents the additive white Gaussian noise.

## B. Channel Model

It is well-known that the narrowband mmWave channel can be characterized by a widely-used Saleh-Valenzuela (S-V) geometric model [32], [33]. As for THz channels, some initial channel measurements at THz frequencies [34]–[37] reported that THz channels also exhibit sparse scattering characteristics, an effect that is observable at mmWave frequencies. The main difference between the mmWave and THz channels lies in the path loss. Specifically, THz channels suffer more severe free spreading loss due to the extremely high frequency. In addition, the high attenuation caused by molecular absorption is no longer negligible and has to be taken into account at THz frequencies. On the other hand, due to the severe path loss of THz frequencies, THz channels may exhibit a higher degree of sparsity than mmWave communications. As a result, THz channels can also be characterized by the S-V model. Specifically, the BS-IRS channel can be modeled as

$$\begin{aligned} \mathbf{G} &= \sqrt{\frac{N_t M}{P}} (\varrho_0 \mathbf{a}_r(\vartheta_0^r, \gamma_0^r) \mathbf{a}_t^H(\phi_0^t) \\ &\quad + \sum_{p=1}^{P-1} \varrho_p \mathbf{a}_r(\vartheta_p^r, \gamma_p^r) \mathbf{a}_t^H(\phi_p^t)) \end{aligned} \quad (4)$$

where  $P$  is the total number of paths between the BS and the IRS,  $\varrho_0$  denotes the complex gain of the LOS path,  $\varrho_p, \forall p = 1, \dots, P-1$  represents the complex gain of the  $p$ th NLOS path,  $\vartheta_p^r(\gamma_p^r)$  for  $p = 0, 1, \dots, P-1$  denotes the associated azimuth (elevation) AoA,  $\phi_p^t$  for  $p = 0, \dots, P-1$  is the associated AoD, and  $\mathbf{a}_r$  ( $\mathbf{a}_t$ ) denotes the normalized receive (transmit) array response vector. For simplicity, we define

$$\mathbf{a}(\phi, N) \triangleq \frac{1}{\sqrt{N}} [1 \ e^{j\pi\phi} \ \dots \ e^{j\pi(N-1)\phi}]^T. \quad (5)$$

Suppose the BS employs a uniform linear array (ULA). The transmit array response vector can be expressed as

$$\mathbf{a}_t(\phi) = \mathbf{a}\left(\frac{2d}{\lambda} \sin \phi, N_t\right). \quad (6)$$

Also, since the IRS is an  $M_y \times M_z$  uniform planar array, the receive array response vector can be written as

$$\mathbf{a}_r(\vartheta, \gamma) = \mathbf{a}\left(\frac{2d}{\lambda} \sin \vartheta \sin \gamma, M_y\right) \otimes \mathbf{a}\left(\frac{2d}{\lambda} \cos \gamma, M_z\right). \quad (7)$$

where  $\otimes$  denotes the Kronecker-product,  $d$  is the antenna spacing and  $\lambda$  denotes the wavelength of the signal.

Owing to the sparse scattering nature of mmWave channels, the BS-IRS channel has a sparse representation in the angular (beam-space) domain:

$$\mathbf{G} = \sqrt{\frac{N_t M}{P}} (\mathbf{D}_{M_y} \otimes \mathbf{D}_{M_z}) \Sigma \mathbf{D}_{N_t}^H = \sqrt{\frac{N_t M}{P}} \mathbf{D}_R \Sigma \mathbf{D}_{N_t}^H \quad (8)$$

where  $\mathbf{D}_R \triangleq \mathbf{D}_{M_y} \otimes \mathbf{D}_{M_z} \in \mathbb{C}^{M \times M}$ ,  $\mathbf{D}_{M_y}$ ,  $\mathbf{D}_{M_z}$ , and  $\mathbf{D}_{N_t}$  are defined as

$$\mathbf{D}_N \triangleq [\mathbf{a}(\eta(1), N), \dots, \mathbf{a}(\eta(N), N)] \in \mathbb{C}^{N \times N}, \quad (9)$$

with  $N = M_y, M_z, N_t$  respectively,  $\eta(i) = -1 + \frac{2i-1}{N}, i = 1, \dots, N$ , and  $\Sigma \in \mathbb{C}^{M \times N_t}$  is a sparse matrix with  $P$  nonzero entries. Here we suppose that the true AoA and AoD lie on the discretized grid. In the presence of grid mismatch, the number of nonzero elements in the sparse matrix will increase as a result of power leakage.

Similarly, the IRS-user channel can be modeled as

$$\mathbf{h}_r = \sqrt{\frac{M}{P'}} \left( \alpha_0 \mathbf{a}_r(\vartheta_0^t, \gamma_0^t) + \sum_{p=1}^{P'-1} \alpha_p \mathbf{a}_r(\vartheta_p^t, \gamma_p^t) \right), \quad (10)$$

where  $P'$  is the number of signal paths between the IRS and the user,  $\alpha_0$  denotes the complex gain of the LOS path,  $\alpha_p, \forall p = 1, \dots, P'-1$  denotes the complex gain associated with the  $p$ th NLOS path, and  $\vartheta_p^t(\gamma_p^t)$  for  $p = 0, 1, \dots, P'-1$  denotes the associated azimuth (elevation) AoD. Due to sparse scattering characteristics, the IRS-user channel can be written as

$$\mathbf{h}_r = \sqrt{\frac{M}{P'}} \mathbf{D}_R \boldsymbol{\alpha}, \quad (11)$$

where  $\boldsymbol{\alpha} \in \mathbb{C}^{M \times 1}$  is a sparse vector with  $P'$  nonzero entries. It is easy to verify that  $\mathbf{D}_R^H \mathbf{D}_R = \mathbf{I}_M$  and  $\mathbf{D}_{N_t}^H \mathbf{D}_{N_t} = \mathbf{I}_{N_t}$ .

Based on (8) and (11), it was shown in [13] that the cascade channel admits a sparse representation as follows

$$\begin{aligned} \mathbf{H} &= \sqrt{\frac{N_t M}{P P'}} \bar{\mathbf{D}}_R \tilde{\Lambda} \mathbf{D}_{N_t}^H \\ &= \bar{\mathbf{D}}_R \Lambda \mathbf{D}_{N_t}^H, \end{aligned} \quad (12)$$

where  $\bar{\mathbf{D}}_R \triangleq \tilde{\mathbf{D}}_R(:, 1:M)$  is a submatrix of  $\tilde{\mathbf{D}}_R$  constructed by its first  $M$  columns, and  $\tilde{\mathbf{D}}_R \triangleq \sqrt{M} \mathbf{D}_R^* \bullet \mathbf{D}_R$ , with  $\bullet$  denoting the transposed Khatri-Rao product. It can be readily verified that  $\tilde{\mathbf{D}}_R \in \mathbb{C}^{M \times M^2}$  has  $M$  distinct columns which are exactly its first  $M$  columns. Also, we can verify that  $\bar{\mathbf{D}}_R$

is an unitary matrix, i.e.  $\bar{\mathbf{D}}_R^H \bar{\mathbf{D}}_R = \mathbf{I}_M$ , and its column takes the form of  $\bar{\mathbf{a}}_r(\varphi, \varpi) \triangleq \mathbf{a}(\varphi, M_y) \otimes \mathbf{a}(\varpi, M_z)$ .

Also, we have

$$\mathbf{\Lambda} \triangleq \sqrt{\frac{N_t M}{P P'}} \tilde{\mathbf{\Lambda}} \in \mathbb{C}^{M \times N_t} \quad (13)$$

in which  $\tilde{\mathbf{\Lambda}}$  is a merged version of  $\mathbf{J} \triangleq \boldsymbol{\alpha}^* \otimes \boldsymbol{\Sigma}$ , with each of its rows being a superposition of a subset of rows in  $\mathbf{J}$ , i.e.

$$\tilde{\mathbf{\Lambda}}(i, :) = \sum_{n \in \mathcal{S}_i} \mathbf{J}(n, :) \quad (14)$$

where  $\tilde{\mathbf{\Lambda}}(i, :)$  denotes the  $i$ th row of  $\tilde{\mathbf{\Lambda}}$ ,  $\mathcal{S}_i$  denotes the set of indices associated with those columns in  $\bar{\mathbf{D}}_R$  that are identical to the  $i$ th column of  $\bar{\mathbf{D}}_R$ . It is clear that  $\mathbf{\Lambda}$  is a sparse matrix with at most  $P \times P'$  nonzero elements.

### C. Problem Formulation

Combining (3) and (12), the received pilot signal at the user can be expressed as

$$\begin{aligned} z(t) &= \mathbf{v}^H(t) \mathbf{H} \mathbf{f}(t) + n(t) \\ &= \mathbf{v}^H(t) \bar{\mathbf{D}}_R \mathbf{\Lambda} \mathbf{D}_{N_t}^H \mathbf{f}(t) + n(t) \end{aligned} \quad (15)$$

Note that (15) is an ideal signal model without considering the CFO and random phase noise. In mmWave/THz bands, the CFO, i.e., the mismatch in the carrier frequencies at the transmitter and the receiver, is more significant than sub-6GHz bands and cannot be neglected. For instance, a small offset of 10 parts per million (ppm) at mmWave frequencies can cause a large phase misalignment in less than a hundred nanoseconds. Besides the CFO, mmWave communication systems also suffer random phase noise due to the jitter of the oscillators. The phase noise, together with the CFO, leads to an unknown phase shift to measurements  $z(t)$  that varies across time. In this case, only the magnitude of the measurement  $z(t)$  is reliable. Define

$$y(t) \triangleq |z(t)| = |\mathbf{v}^H(t) \bar{\mathbf{D}}_R \mathbf{\Lambda} \mathbf{D}_{N_t}^H \mathbf{f}(t) + n(t)| \quad (16)$$

Based on  $\{y(t)\}_{t=1}^T$ , our objective is to acquire the information needed to achieve beam alignment between the BS and the user. Note that identifying the best beam alignment is equivalent to acquiring the location index of the largest (in magnitude) element in the sparse matrix  $\mathbf{\Lambda}$ . This is because  $\mathbf{\Lambda}$  is a beam-space representation of the cascade channel  $\mathbf{H}$ . Hence the largest element in  $\mathbf{\Lambda}$  actually corresponds to the strongest path of the BS-IRS-user channel.

To identify the largest element in  $\mathbf{\Lambda}$ , a natural approach is to exhaustively search all possible beam pairs. Specifically, at each time instant  $t$ , choose  $\mathbf{f}(t) \triangleq \mathbf{F}_{\text{RF}}(t) \mathbf{f}_{\text{BB}}(t)$  as a certain column from  $\mathbf{D}_{N_t}$ , and choose  $\mathbf{v}(t)$  as a certain column from  $\bar{\mathbf{D}}_R$ , i.e.

$$\mathbf{v}(t) = \sqrt{M} \bar{\mathbf{D}}_R(:, i), \quad (17)$$

$$\mathbf{f}(t) = \mathbf{D}_{N_t}(:, j), \quad (18)$$

Here the scalar  $\sqrt{M}$  in  $\mathbf{v}(t)$  is used to ensure that entries of  $\mathbf{v}(t)$  are of constant modulus. Then the received measurement  $y(t)$  is given by

$$y(t) = |\sqrt{M} \lambda_{i,j} + n(t)| \quad (19)$$

where  $\lambda_{i,j}$  denotes the  $(i, j)$ th entry of  $\mathbf{\Lambda}$ . After an exhaustive search, we can identify the largest (in magnitude) entry in  $\mathbf{\Lambda}$ . This exhaustive search scheme, however, has a sample complexity of  $M N_t$ , which is prohibitively high since both  $M$  and  $N_t$  are large for mmWave and THz systems in order to combat severe path loss. In the following sections, we develop a more efficient method to perform joint BS-IRS-user beam training.

Specifically, since the period of time for beam training is proportional to the number of measurements  $T$ , the problem of interest is how to devise the active/passive beam training sequences  $\{\mathbf{f}(t), \mathbf{v}(t)\}_{t=1}^T$  and develop a computationally efficient estimation scheme such that we can identify the best beam alignment using as few measurements as possible.

*Remark:* Different from our work that neglects the phase information of the received measurements, we noticed that some other works, e.g. [17], [18], model the CFO as an unknown parameter and perform joint CFO and channel estimation.

### III. BEAM TRAINING SEQUENCE DESIGN

To more efficiently probe the channel, we propose to let the BS and the IRS form multiple pencil beams simultaneously and steer them towards different directions. Specifically, the precoding vector  $\mathbf{f}(t)$  is chosen to be

$$\mathbf{f}(t) = \mathbf{F}_{\text{RF}}(t) \mathbf{f}_{\text{BB}}(t) = \mathbf{D}_{N_t} \mathbf{S}(t) \mathbf{f}_{\text{BB}}(t) = \mathbf{D}_{N_t} \mathbf{a}(t), \quad (20)$$

where  $\mathbf{S}(t) \in \{0, 1\}^{N_t \times R}$  is a column selection matrix which has only one nonzero element in each column and  $\mathbf{a}(t) \triangleq \mathbf{S}(t) \mathbf{f}_{\text{BB}}(t)$  is a sparse vector with at most  $R$  nonzero entries. Note that each column of  $\mathbf{D}_{N_t}$  can be considered as a beamforming vector steering a beam to a certain direction. Hence, the hybrid precoding vector in (20) can form at most  $R$  beams towards different directions simultaneously. The passive reflecting vector  $\mathbf{v}(t)$  can be generated in a similar way. We let

$$\mathbf{v}(t) = \bar{\mathbf{D}}_R \mathbf{c}(t), \quad (21)$$

where  $\mathbf{c}(t)$  is a sparse vector containing at most  $Q$  nonzero elements. Here  $Q$  is a parameter of user's choice. We will discuss its choice later in this paper.

Substituting (20)-(21) into (16), we obtain

$$y(t) = |\mathbf{c}^H(t) \mathbf{\Lambda} \mathbf{a}(t) + n(t)| \quad (22)$$

#### A. Sensing Matrix Design

In this subsection, we discuss how to devise a set of sparse sensing vectors  $\{\mathbf{c}(t), \mathbf{a}(t)\}_{t=1}^T$  to efficiently probe the channel. Let  $\mathcal{S}_c(t) \triangleq \{i | c_i(t) > 0\}$  denote the set of indices associated with the nonzero elements in  $\mathbf{c}(t)$ , and  $\mathcal{S}_a(t) \triangleq \{j | a_j(t) > 0\}$  denote the set of indices of the nonzero elements in  $\mathbf{a}(t)$ . Also, for simplicity, we assume that the nonzero entries in  $\{\mathbf{c}(t)\}$  are all set to  $\beta > 0$ , and the nonzero entries in  $\{\mathbf{a}(t)\}$  are all set to  $\gamma > 0$ . Therefore, we have

$$y(t) = |\beta \gamma \sum_{i \in \mathcal{S}_c(t), j \in \mathcal{S}_a(t)} \lambda_{i,j} + n(t)| \quad (23)$$

To find the strongest signal path, we need to make sure that each element in  $\Lambda$  will be scanned at least once. We first introduce the concept of ‘‘a round of full-coverage scanning’’ as a basic building block for our beam training process. Define  $U \triangleq M/Q$  and  $V \triangleq N_t/R$  and assume both of them are integers. Each round of full-coverage scanning consists of  $T_0 = U \times V$  measurements, and these  $T_0$  measurements are generated according to:

$$\mathbf{Y} = |\mathbf{C}^H \Lambda \mathbf{A} + \mathbf{N}| \quad (24)$$

where  $\mathbf{C} \in \mathbb{R}^{M \times U}$ ,  $\mathbf{A} \in \mathbb{R}^{N_t \times V}$ , and  $\mathbf{Y} \in \mathbb{R}^{U \times V}$  is a matrix constructed by  $\{y(t)\}_{t=1}^{T_0}$ . Specifically, the  $(u, v)$ th entry of  $\mathbf{Y}$  is equal to  $\mathbf{Y}(u, v) = y((u-1)V + v)$ , and  $(u, v)$ th entry of  $\mathbf{N}$  is equal to  $\mathbf{N}(u, v) = n((u-1)V + v)$ . Therefore, once  $\mathbf{C}$  and  $\mathbf{A}$  are specified, the set of sparse sensing vectors  $\{\mathbf{c}(t), \mathbf{a}(t)\}_{t=1}^{T_0}$  can be accordingly determined. Let

$$\begin{aligned} \mathbf{C} &= [\mathbf{c}_1 \ \mathbf{c}_2 \ \dots \ \mathbf{c}_U] \\ \mathbf{A} &= [\mathbf{a}_1 \ \mathbf{a}_2 \ \dots \ \mathbf{a}_V] \end{aligned} \quad (25)$$

From the relation between  $\mathbf{Y}$  and  $\{y(t)\}$ , it is clear that we have  $\mathbf{c}_u = \mathbf{c}((u-1)V + v), \forall v$  and  $\mathbf{a}_v = \mathbf{a}((u-1)V + v), \forall u$ . The set of sparse encoding vectors  $\{\mathbf{c}_u\}$  and  $\{\mathbf{a}_v\}$  are devised to satisfy the following two conditions:

- C1 Those nonzero entries in  $\{\mathbf{c}_u\}$  and  $\{\mathbf{a}_v\}$  are respectively set to  $\beta$  and  $\gamma$ . Also, we have  $\|\mathbf{c}_u\|_0 = Q, \forall u$ , and  $\|\mathbf{a}_v\|_0 = R, \forall v$ .
- C2 The sparse vectors in  $\{\mathbf{c}_u\}$  are orthogonal to each other, i.e.  $\mathbf{c}_{u_1}^T \mathbf{c}_{u_2} = 0, \forall u_1 \neq u_2$ ; and vectors in  $\{\mathbf{a}_v\}$  are orthogonal to each other, i.e.  $\mathbf{a}_{v_1}^T \mathbf{a}_{v_2} = 0, \forall v_1 \neq v_2$ .

Let  $S(t) \triangleq \{\lambda_{i,j}\}_{i \in S_c(t), j \in S_a(t)}$  denote the set of elements that are simultaneously sensed/hashed at the  $t$ th time instant. Such a set of elements is also called as a bin, as illustrated in Fig. 3. Clearly we have  $|S(t)| = QR$ . Also, condition C2 ensures that the sets of elements sensed at different time instants are disjoint, i.e.

$$S(t_1) \cap S(t_2) = \emptyset, \forall t_1 \neq t_2 \quad (26)$$

In addition, since we have  $UQ = M$  and  $RV = N_t$ , the union of the sets is equal to the whole set of elements of  $\Lambda$ , i.e.

$$S(1) \cup \dots \cup S(T_0) = \{\lambda_{i,j}\}_{i=1, j=1}^{i=M, j=N_t} \quad (27)$$

After a single round of full-coverage scanning, no element in  $\Lambda$  is left unscanned. Nevertheless, since each element in  $\Lambda$  is scanned along with other elements at each time, we still cannot identify the exact location of the largest component from the measurements  $\mathbf{Y}$ . To identify the strongest component, we need to perform a few rounds, say  $L$  rounds, of full-coverage scanning, and for each round of scanning, we randomly generate  $\mathbf{A}$  and  $\mathbf{C}$  by altering locations of the nonzero entries in  $\{\mathbf{c}_u\}$  and  $\{\mathbf{a}_v\}$ . We will show that we can identify the largest element in  $\Lambda$  via a simple decoding scheme from these  $L$  rounds of measurements  $\{\mathbf{Y}_l\}_{l=1}^L$ . Here  $\mathbf{Y}_l$  denotes the measurement matrix collected at the  $l$ th round of scanning, and we have

$$\mathbf{Y}_l = |\mathbf{C}_l^H \Lambda \mathbf{A}_l + \mathbf{N}_l| \quad (28)$$

where  $\mathbf{C}_l \triangleq [\mathbf{c}_1^l \ \dots \ \mathbf{c}_U^l]$  and  $\mathbf{A}_l \triangleq [\mathbf{a}_1^l \ \dots \ \mathbf{a}_V^l]$  are sparse encoding matrices used in the  $l$ th round of scanning.

## B. Practical Considerations of Devising $\{\mathbf{c}_u\}$

As discussed in the previous subsection, the vectors  $\{\mathbf{c}_u\}$  are devised to be strictly sparse with  $Q$  nonzero elements. To fulfill this requirement, we need to have an independent control of the reflection amplitude for each IRS element, which increases not only the hardware complexity but also the energy consumption [38], [39]. Moreover, to generate a strictly sparse vector  $\mathbf{c}_u$ , many of the reflection amplitudes have to be set far less than one, which reduces the reflection efficiency.

To cope with these issues, we wish to find a set of passive beamforming vectors  $\{\mathbf{v}_u\}$  with constant modulus, and the corresponding vectors  $\{\mathbf{c}_u = \bar{\mathbf{D}}_R^H \mathbf{v}_u\}$  are approximately-sparse vectors with  $Q$  dominant entries. Mathematically, this problem can be formulated as follows. Given any  $Q$  columns from  $\bar{\mathbf{D}}_R$ , denoted as  $\{\mathbf{p}_q\}_{q=1}^Q$ , let  $\mathbf{Q}$  be a matrix constructed by these  $Q$  columns and  $\bar{\mathbf{Q}}$  be a matrix obtained by removing those  $Q$  columns from  $\bar{\mathbf{D}}_R$ . We seek a constant-modulus vector  $\mathbf{v}$  such that  $|\mathbf{v}^H \mathbf{Q}|$  is a quasi-constant magnitude vector with its magnitude as large as possible, whereas  $\|\mathbf{v}^H \bar{\mathbf{Q}}\|_2$  is as small as possible. There are different approaches to tackle this problem. Inspired by [6], here we formulate the above problem into the following optimization:

$$\begin{aligned} \max_{\mathbf{v}} \quad & \sum_{q=1}^Q \log_2(1 + \mathbf{v}^H \mathbf{p}_q \mathbf{p}_q^H \mathbf{v}) \\ \text{s.t.} \quad & |v_i| = 1, \forall i = 1, \dots, M \end{aligned} \quad (29)$$

where  $v_i$  denotes the  $i$ th entry of the vector  $\mathbf{v}$ . It was shown in [6] that the solution to (29) is nearly orthogonal to  $\bar{\mathbf{Q}}$ . Moreover, entries of the vector  $\mathbf{v}^H \mathbf{Q}$  have quasi-constant magnitudes thanks to the logarithmic function. As a result, the resulting vector  $\mathbf{c} = \bar{\mathbf{D}}_R^H \mathbf{v}$  is an approximately sparse vector with  $Q$  dominant entries. Note that the generated vectors  $\{\mathbf{c}_u\}$  cannot be strictly orthogonal to each other since they are no longer strictly sparse vectors. Nevertheless, for each round of full-coverage scanning, it is not difficult to attain near-orthogonality by making sure that the sets of dominant elements sensed at different time instants are disjoint. Also, as will be shown later in this paper, our proposed algorithm requires the indices of those nonzero elements in  $\{\mathbf{c}_u\}$  to identify the best alignment. As  $\{\mathbf{c}_u\}$  generated from (29) are approximately sparse, we only consider these  $Q$  prominent entries as nonzero elements of  $\mathbf{c}_u$ .

The above optimization can be efficiently solved by a manifold-based algorithm, which has a very low computational complexity of  $\mathcal{O}(M)$  [6]. Besides, the reflecting vectors  $\{\mathbf{v}_u\}$  can be calculated and stored in advance. It will not exert an extra computational burden on the beam alignment task.

## IV. PROPOSED BEAM ALIGNMENT METHOD: LOS SCENARIOS

In the previous section, we have discussed how to devise the active and passive beam training sequences  $\{\mathbf{f}(t)\}_{t=1}^T$  and  $\{\mathbf{v}(t)\}_{t=1}^T$ . In this section, we discuss how to identify the best beam alignment (i.e., identify the largest element in  $\Lambda$ ) from the received phaseless measurements  $\{y(t)\}_{t=1}^T$  for the LOS

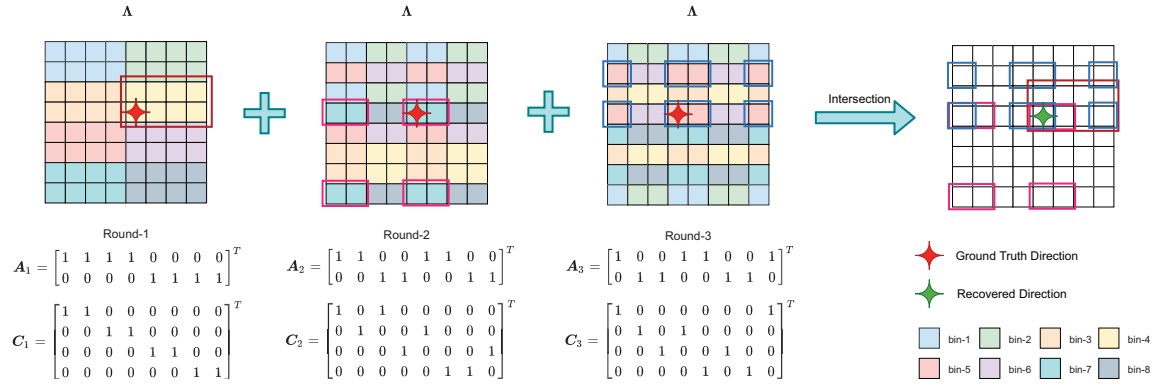


Fig. 3. An illustrative example to show how the proposed scheme recovers the location of the largest element in  $\Lambda$ . A bin consists of those entries in  $\Lambda$  that are simultaneously sensed at each time instant. For different rounds, we randomize the entries that fall into different bins. In each round, the bin associated with the largest measurement  $y(t)$  is highlighted with a rectangular box. By performing the intersection operation, the entry associated with the dominant path can be estimated as the common element of those rectangular boxes.

scenario. Note that this estimation task is performed at the receiver, i.e. user.

We first consider the scenario where there is only one nonzero element or only one prominent nonzero element in the matrix  $\Lambda$ . This scenario has important practical implications and arises as a result when both the BS-IRS channel and the IRS-user channel are LOS-dominated. As reported in many real-world channel measurements [40], [41], the power of mmWave LOS path is much higher (about 13 dB higher) than the sum of the power of NLOS paths. When it comes to the THz bands, the power of the LOS component is about 20dB higher than the power of the scattering components [42]. Therefore it can be expected that  $\Lambda$  contains only one dominant element when the LOS path is available for both the BS-IRS and the IRS-user links.

To better illustrate the idea of the proposed scheme, we consider a noiseless case where the measurements  $\{\mathbf{Y}_l\}$  are not corrupted by noise. When  $\Lambda$  contains only one dominant element, it is clear that the measurement matrix  $\mathbf{Y}_l$  collected at the  $l$ th round of scanning contains only one prominent component whose location can be easily determined. Suppose that, for each  $l$ ,  $\mathbf{Y}_l(u_l, v_l)$  is the largest element in  $\mathbf{Y}_l$ . From (28), we have

$$\mathbf{Y}_l(u_l, v_l) = (\mathbf{c}_{u_l}^l)^H \Lambda \mathbf{a}_{v_l}^l \quad (30)$$

Let  $S_{u_l}^{(l)} \triangleq \{i | \mathbf{c}_{u_l}^l(i) > 0\}$  denote the indices of the nonzero elements in  $\mathbf{c}_{u_l}^l$ , and  $S_{v_l}^{(l)} \triangleq \{j | \mathbf{a}_{v_l}^l(j) > 0\}$  denote the indices of the nonzero elements in  $\mathbf{a}_{v_l}^l$ .

Let  $(i^*, j^*)$  denote the location index of the dominant entry in  $\Lambda$ . It is clear that we have

$$i^* \in S_{u_l}^{(l)}, \quad j^* \in S_{v_l}^{(l)}, \quad \forall l \quad (31)$$

As a result, we have

$$i^* \in \bigcap_{l=1}^L S_{u_l}^{(l)} \quad j^* \in \bigcap_{l=1}^L S_{v_l}^{(l)} \quad (32)$$

On the other hand, since  $\mathbf{c}_{u_l}^l$  and  $\mathbf{a}_{v_l}^l$  are randomly generated for each round of scanning, it is unlikely that there exists another location index  $(i, j)$  which lies in the intersection of

these sets, particularly when  $L$  is large. Therefore we can determine the location index of the dominant entry,  $(i^*, j^*)$ , as

$$i^* = \bigcap_{l=1}^L S_{u_l}^{(l)} \quad j^* = \bigcap_{l=1}^L S_{v_l}^{(l)} \quad (33)$$

In Fig. 3, we provide an illustrative example to show how to identify the largest element via an intersection scheme.

Our following theorem shows that such an intersection scheme can recover the true location of the dominant element with a high probability. The main results are summarized as follows.

*Theorem 1:* Suppose  $Q < M$  and  $R < N_t$ . After  $L$  rounds of full-coverage scanning, from (33), we can identify the location of the nonzero element in  $\Lambda$  with a probability greater than

$$P \geq \left(1 - (M-1) \left(\frac{Q-1}{M-1}\right)^L\right) \times \left(1 - (N_t-1) \left(\frac{R-1}{N_t-1}\right)^L\right) \\ = P(Q, L, M) \times P(R, L, N_t) \quad (34)$$

where the function  $P(x, y, z)$  is defined as

$$P(x, y, z) \triangleq 1 - (z-1) \left(\frac{x-1}{z-1}\right)^y \quad (35)$$

*Proof:* See Appendix A. ■

#### A. Sample Complexity Analysis

We now analyze the sample complexity of the proposed scheme. To ensure that we can recover the index of the dominant element of  $\Lambda$  with a probability exceeding a predefined threshold  $p_0$ , we need

$$P \geq P(Q, L, M) \times P(R, L, N_t) \geq p_0 \quad (36)$$

For simplicity, we set  $p_0 = p_1 \times p_2$ , and let

$$P(Q, L, M) \geq p_1 \quad (37)$$

$$P(R, L, N_t) \geq p_2 \quad (38)$$

From (37), it is easy to verify that

$$L \geq \frac{\log \frac{1-p_1}{M-1}}{\log \frac{Q-1}{M-1}} = \frac{\log(M-1) + c_1}{\log \frac{M-1}{Q-1}} \triangleq L_1 \quad (39)$$

where  $c_1 \triangleq \log((1-p_1)^{-1}) > 0$  is a constant. On the other hand, from (38), we have

$$L \geq \frac{\log \frac{1-p_2}{N_t-1}}{\log \frac{R-1}{N_t-1}} = \frac{\log(N_t-1) + c_2}{\log \frac{N_t-1}{R-1}} \triangleq L_2 \quad (40)$$

where  $c_2 = \log((1-p_2)^{-1})$  is a constant.

Therefore, the total number of measurements  $T$  required for identifying the strongest component with a probability at least  $p_0$  can be calculated as

$$T = UVL \geq UV \max\{L_1, L_2\} \quad (41)$$

Since  $L_1$  ( $L_2$ ) is in the order of  $\mathcal{O}(\log(M))$  ( $\mathcal{O}(\log(N_t))$ ), the proposed intersection-based scheme has a sample complexity of  $\mathcal{O}(UV \max\{\log(M), \log(N_t)\})$ . Recall that  $U = M/Q$ , where  $Q$  is a parameter of user's choice. Thus, we can choose a proper  $Q$  to obtain a small value of  $U$ . To be specific, given  $T$  and other system parameters, we can try different combinations of  $(Q, L)$  to determine the one which yields the highest probability of correct beam alignment. Here we provide an example to show how many measurements are exactly required to achieve perfect beam alignment with a decent probability. Suppose  $N_t = 128$ ,  $M = 256$ ,  $R = 4$ . For different choice of  $Q$  and  $L$ , our proposed method can identify the best beam alignment with a probability no less than:

- $Q = 32$ ,  $L = 4$ ,  $T = UVL = 1024$ :  $P \geq 94.43\%$
- $Q = 16$ ,  $L = 3$ ,  $T = UVL = 1536$ :  $P \geq 94.65\%$
- $Q = 16$ ,  $L = 4$ ,  $T = UVL = 2048$ :  $P \geq 99.69\%$

From this example, we see that the proposed scheme can achieve a substantial training overhead reduction as compared with the exhaustive search scheme which requires a total number of measurements up to  $T = MN_t = 32768$ .

### B. Extension To The Noisy Case

The proposed intersection scheme may not work well in the presence of noise. In the sequel, inspired by [24], we develop a noisy version of the intersection scheme. The basic idea is to assign each element in  $\mathbf{\Lambda}$  a probability instead of a 0/1-hard vote, and turn the intersection operation into a product of probabilities.

Specifically, for each round of scanning and each index  $(i, j)$  of the element in  $\mathbf{\Lambda}$ , we define an indicator matrix,  $\mathbf{I}_{(i,j)}^{(l)} \in \{0, 1\}^{U \times V}$ , with its  $(u, v)$ th entry defined as

$$\mathbf{I}_{(i,j)}^{(l)}(u, v) \triangleq \begin{cases} 1 & \text{if } \mathbf{c}_u^l(i) \times \mathbf{a}_v^l(j) \neq 0 \\ 0 & \text{otherwise.} \end{cases} \quad (42)$$

where  $\mathbf{x}(j)$  denotes the  $j$ th element of the vector  $\mathbf{x}$ . Clearly, if the element  $\mathbf{\Lambda}(i, j)$  is sensed at the time instant  $((u-1)V + v)$  of the  $l$ th round, the value in (42) would be 1; otherwise it would be 0.

Based on the indicator matrix, we can further calculate the ‘‘probability’’ matrix  $\mathcal{P}^{(l)}$  with its  $(i, j)$ th entry defined as

$$\mathcal{P}^{(l)}(i, j) \triangleq \left( \text{vec}(\mathbf{I}_{(i,j)}^{(l)}) \right)^T \text{vec}(\mathbf{Y}_l \circ \mathbf{Y}_l^*) \quad (43)$$

where  $\text{vec}(\cdot)$  denotes the vectorization operator and  $\circ$  represents the Hadamard product. Here (43) uses the received magnitude measurement as a weight to calculate the probability of the element  $\mathbf{\Lambda}(i, j)$  being a dominant entry in  $\mathbf{\Lambda}$ .

Generally, if  $\mathcal{P}^{(l)}(i, j) \geq \epsilon$ , where  $\epsilon$  is a pre-specified threshold, then  $(i, j)$  is regarded as a candidate index of the dominant entry in  $\mathbf{\Lambda}$ . Let  $\mathcal{F}_l = \{(i, j) | \mathcal{P}^{(l)}(i, j) \geq \epsilon\}$  denote the set of candidate indices obtained from the  $l$ th round. After  $L$  rounds of scanning, we can determine the location index of the dominant entry  $(i^*, j^*)$  via a maximum likelihood (ML) estimation

$$(i^*, j^*) = \max_{(i,j) \in \mathcal{F}} \prod_{l=1}^L \mathcal{P}^{(l)}(i, j) \quad (44)$$

where  $\mathcal{F} \triangleq \cup_{l=1}^L \mathcal{F}_l$  denotes the set comprising all candidate indices. The overall algorithm for LOS scenarios are summarized in Algorithm 1.

---

### Algorithm 1 Proposed beam alignment algorithm for LOS scenarios

---

- 1: Generate  $\{\mathbf{A}_l\}_{l=1}^L$  according to Section III.A;
  - 2: Generate  $\{\mathbf{C}_l\}_{l=1}^L$  according to Section III.B;
  - 3: Obtain received signals  $\{\mathbf{Y}_l\}_{l=1}^L$  for  $L$  rounds;
  - 4: **for**  $l = 1, \dots, L$  **do**
  - 5:   Calculate the ‘‘probability’’ function via (43) for all indices  $(i, j)$ .
  - 6: **end for**
  - 7: Determine the best beam direction index  $(i^*, j^*)$  of the dominant element in  $\mathbf{\Lambda}$  via (44).
- 

### C. Computational Complexity Analysis

The major computational task of our proposed beam estimation method is to calculate the probability matrix defined in (43). According to (43), each entry of the probability matrix is calculated as an inner product of two  $UV$ -dimensional vectors. Since each element in  $\mathbf{\Lambda}$  is sensed only once in each round, the indicator matrix  $\mathbf{I}_{(i,j)}^{(l)}$  contains only one nonzero entry. Therefore each entry of the probability matrix can be calculated by multiplying this nonzero entry with its corresponding entry in  $\text{vec}(\mathbf{Y}_l \circ \mathbf{Y}_l^*)$ . As a result, calculating this entire probability matrix  $\mathcal{P}^{(l)} \in \mathbb{R}^{M \times N_t}$  involves a computational complexity of  $\mathcal{O}(MN_t)$ . Note that our proposed method requires to compute a set of probability matrices  $\{\mathcal{P}^{(l)}\}_{l=1}^L$ , which has a computational complexity in the order of  $\mathcal{O}(MN_tL)$ , where  $L$  is the number of rounds of full-coverage scanning. After obtaining  $\{\mathcal{P}^{(l)}\}_{l=1}^L$ , we need to calculate the objective function defined in (44), which is a Hadamard product of the set of probability matrices  $\{\mathcal{P}^{(l)}\}_{l=1}^L$  and involves a computational complexity of  $\mathcal{O}(MN_t(L-1))$ . From the above discussion, we see that the overall computational complexity of our proposed method is in the order of  $\mathcal{O}(MN_tL)$ .

As a comparison, as analyzed in [13], if we employ a compressed sensing-based method to recover the cascade channel, the method needs to solve a sparse signal recovery problem of size  $T \times (MN_t)$ , whose computational complexity is of  $\mathcal{O}(MN_t T \bar{K})$  for greedy methods and of  $\mathcal{O}(M^3 N_t^3)$  for more sophisticated methods such as the basis pursuit. Here  $T$  denotes the number of measurements used for channel estimation, and  $\bar{K}$  is the sparsity level of the cascade channel matrix. Our analysis shows that for our proposed method, only a few rounds of full-coverage scanning (say,  $L < 10$ ) are sufficient to identify the best beam alignment with a probability close to 1. Hence generally we have  $L \ll T \bar{K}$ . Therefore, our proposed method has a much lower complexity even compared with the least computationally demanding compressed sensing method.

## V. PROPOSED BEAM ALIGNMENT METHOD FOR NLOS SCENARIOS

In this section, we extend our proposed method to a more general case where there are multiple comparable nonzero elements in the sparse matrix  $\Lambda$ . Such a scenario arises as a result of NLOS transmissions when either the BS-IRS's LOS path or the IRS-user's LOS path is blocked by obstacles. For the case where multiple paths of comparable qualities are available from the BS to the user, the signals from different paths may combine destructively at the receiver, thus creating difficulties to identify the strongest path. Due to this destructive multi-path effect, a direct application of the above proposed method may result in beam misalignment. To address this issue, we propose a modified version of the set intersection-based method for identifying the strongest component in  $\Lambda$ .

We first consider a noiseless case to illustrate the idea of the proposed estimation scheme. Recalling (23), we have

$$y(t) = \left| \beta \gamma \sum_{S(t)} \lambda_{i,j} \right| \quad (45)$$

where  $S(t) = \{\lambda_{i,j}\}_{i \in S_c(t), j \in S_a(t)}$  denotes the set of elements that are simultaneously sensed at the  $t$ th time instant. According to the number of nonzero elements in the set  $S(t)$ , the associated received signal  $y(t)$  is called as a nullton, a singleton, and a multiton if:

- Nullton: The received signal  $y(t)$  is a nullton if its associated set  $S(t)$  contains no nonzero element.
- Singleton: The received signal  $y(t)$  is a singleton if its associated set  $S(t)$  includes only a single nonzero element.
- Multiton: The received signal  $y(t)$  is a multiton if its associated set  $S(t)$  includes more than one nonzero elements.

Also, if the measurements collected within a certain round of scanning, say  $\mathbf{Y}_l$ , only contain singleton and nullton measurements, then this round of scanning is referred to as a no-multiton (NM) round.

The basic idea of our proposed scheme is to utilize the measurements associated with those NM rounds of scanning to identify the largest component in  $\Lambda$ . Since the NM rounds consist of only singleton and nullton measurements, it means

that signals from different paths are separately sensed and will not be hashed to contribute to a same measurement. Thus the signals from different paths will not be combined destructively at the receiver.

Nevertheless, we first need to differentiate NM rounds from those rounds of scanning which include multiton measurements. Suppose that the sparse matrix  $\Lambda$  contains  $K$  nonzero elements, where  $K \ll MN_t$ . Recall that for each round of scanning, the sets of elements sensed at different time instants are disjoint, i.e.  $S(t_1) \cap S(t_2) = \emptyset, \forall t_1 \neq t_2$ , and the union of the sets is the whole set of elements of  $\Lambda$ , i.e.  $S(1) \cup \dots \cup S(T) = \{\lambda_{i,j}\}_{i=1, j=1}^{i=M, j=N_t}$ . Therefore for an NM round, it should contain exactly  $K$  singleton measurements and  $UV - K$  nullton measurements. On the other hand, if a round of scanning is not an NM round, then it should include more than  $UV - K$  nullton measurements because some of the  $K$  nonzero elements in  $\Lambda$  are sensed simultaneously. Motivated by this observation, we can consider those rounds with the smallest number of nulltons as NM rounds, without assuming the knowledge of  $K$ . Note that determining whether  $y(t)$  is a nullton measurement or not is simple in the noiseless case because we have  $y(t) = 0$  if  $y(t)$  is a nullton. In the noisy case, an energy detector can be employed to differentiate nulltons from singletons and multitons.

After those NM rounds are identified, we can employ the intersection-based scheme to find the strongest component in  $\Lambda$ . Suppose there are  $\bar{L}$  NM rounds among all  $L$  rounds, and denote the set of NM rounds as  $\mathcal{L}$ . Suppose that, for each  $l \in \mathcal{L}$ ,  $\mathbf{Y}_l(u_l, v_l)$  is the largest (in magnitude) element in  $\mathbf{Y}_l$ . From (28), we have

$$\mathbf{Y}_l(u_l, v_l) = (\mathbf{c}_{u_l}^l)^H \Lambda \mathbf{a}_{v_l}^l \quad (46)$$

Let  $S_{u_l}^{(l)} \triangleq \{i | \mathbf{c}_{u_l}^l(i) > 0\}$  denote the indices of the nonzero elements in  $\mathbf{c}_{u_l}^l$ , and  $S_{v_l}^{(l)} \triangleq \{j | \mathbf{a}_{v_l}^l(j) > 0\}$  denote the indices of the nonzero elements in  $\mathbf{a}_{v_l}^l$ . Let  $(i^*, j^*)$  denote the location index of the largest (in magnitude) component in  $\Lambda$ . It is clear that we have

$$i^* \in S_{u_l}^{(l)}, \quad j^* \in S_{v_l}^{(l)}, \quad \forall l \in \mathcal{L} \quad (47)$$

As a result, we can estimate  $(i^*, j^*)$  as

$$i^* = \bigcap_{l \in \mathcal{L}} S_{u_l}^{(l)} \quad j^* = \bigcap_{l \in \mathcal{L}} S_{v_l}^{(l)} \quad (48)$$

### A. Theoretical Analysis

From the above discussion, we see that our proposed method relies on those measurements collected within the NM rounds of scanning to find the best beam alignment. A natural question is: how likely a round of full-coverage scanning is an NM-round of scanning? We have the following results regarding this question.

*Proposition 1:* Suppose the location indices of the  $K$  nonzero components in  $\Lambda \in \mathbb{C}^{M \times N_t}$  are uniformly distributed. The sparse encoding matrices  $\mathbf{C}_l \in \{0, 1\}^{M \times U}$  and  $\mathbf{A}_l \in \{0, 1\}^{N_t \times V}$  for the  $l$ th round of scanning are designed to satisfy conditions C1 and C2. Let  $E$  denote the event that

the  $l$ th round of scanning is an NM round. Then we have

$$P(E) = (RQ)^K \frac{\binom{UV}{K}}{\binom{MN_t}{K}} \triangleq p, \quad (49)$$

where  $R = N_t/V$ , and  $Q = M/U$ .

*Proof:* This result is an extension of Proposition 1 in [26]. The proof is thus omitted here. ■

Here we provide an example to show the probability of a round of full-coverage scanning being an NM-round of scanning. Suppose  $N_t = 128$ ,  $M = 256$ , and  $R = 4$ . For different values of  $Q$  and  $K$ , we have

- $Q = 64$ ,  $K = 4$ :  $p = 95.40\%$
- $Q = 32$ ,  $K = 4$ :  $p = 97.69\%$
- $Q = 32$ ,  $K = 2$ :  $p = 99.61\%$

We see that with a reasonable choice of  $Q$ , the measurement matrix  $\mathbf{Y}_l$  is very likely to contain only singleton and nullton measurements. Hence after a few rounds of scanning, it can be expected that most of these rounds of scanning are NM rounds.

Based on Proposition 1, the probability with which the set-intersection estimator (48) can find the largest (in magnitude) element in  $\mathbf{\Lambda}$  can be characterized as follows.

*Theorem 2:* Suppose there are  $1 < K \ll MN_t$  nonzero elements in the sparse matrix  $\mathbf{\Lambda}$ . After  $L$  rounds of full-coverage scanning, from (48), the proposed method can identify the location of the largest element in  $\mathbf{\Lambda}$  with a probability  $P'$  that can be bounded as

$$P' \geq \sum_{l=0}^L g(Q, l, M) \times g(R, l, N_t) \times \binom{L}{l} p^l (1-p)^{L-l} \quad (50)$$

where  $p$  is defined in (49) and the function  $g(Q, l, M)$  is defined as

$$g(Q, l, M) \triangleq 1 - \sum_{j=1}^{Q-1} (-1)^{(j-1)} \binom{M-1}{j} \left( \frac{\binom{M-1-j}{Q-1-j}}{\binom{M-1}{Q-1}} \right)^l. \quad (51)$$

*Proof:* See Appendix B. ■

Here we provide an example to show the probability (50) of identifying the largest component in  $\mathbf{\Lambda}$ . Suppose  $N_t = 128$ ,  $M = 256$ , and  $R = 4$ . For different values of  $Q$ ,  $K$  and  $L$ , we have

- $Q = 32$ ,  $K = 4$ ,  $L = 4$ ,  $T = 1024$ :  $P' \geq 91.52\%$
- $Q = 32$ ,  $K = 4$ ,  $L = 5$ ,  $T = 1280$ :  $P' \geq 98.63\%$
- $Q = 16$ ,  $K = 2$ ,  $L = 4$ ,  $T = 2048$ :  $P' \geq 99.65\%$

Compared this example with the one in Section IV.B, we can see that the proposed method for the NLOS scenario can achieve a decent probability of exact recovery with a sample complexity similar to (or slightly higher than) that of the LOS scenario.

### B. Extension To The Noisy Case

We now extend our proposed estimation method to the noisy case. When the measurements are corrupted by noise, the received signal can be expressed as

$$\mathbf{Y}_l(u, v) = |(\mathbf{c}_u^l)^H \mathbf{\Lambda} \mathbf{a}_v^l + n_{uv}^l| \quad \forall u, v \quad (52)$$

where  $n_{uv}^l \sim \mathcal{CN}(0, \sigma^2)$  denotes the additive noise. We first need to determine whether  $\mathbf{Y}_l(u, v)$  is a nullton measurement or not. Such a problem can be formulated as a binary hypothesis test problem:

$$\begin{aligned} H_0 : \mathbf{Y}_l(u, v) &= |n_{uv}^l|, \\ H_1 : \mathbf{Y}_l(u, v) &= \left| \beta\gamma \sum_{i \in S_u^{(l)}, j \in S_v^{(l)}} \lambda_{i,j} + n_{uv}^l \right| \end{aligned} \quad (53)$$

where  $S_u^{(l)} \triangleq \{i | \mathbf{c}_u^l(i) > 0\}$  denote the indices of the nonzero elements in  $\mathbf{c}_u^l$ , and  $S_v^{(l)} \triangleq \{j | \mathbf{a}_v^l(j) > 0\}$  denote the indices of the nonzero elements in  $\mathbf{a}_v^l$ . A simple energy detector can be used to perform the detection

$$\mathbf{Y}_l(u, v) \underset{H_0}{\overset{H_1}{\geq}} \epsilon \quad (54)$$

Given a specified false alarm probability, the threshold  $\epsilon$  can be easily determined since  $\mathbf{Y}_l(u, v)$  follows a Rayleigh distribution under  $H_0$ . Since the received signals are corrupted by noise, the selection of  $\epsilon$  can result in different performance. To harness the advantage of multiple full-coverage scanning rounds, we often set  $\epsilon$  to be a small value. Next, we choose those rounds of scanning with the least number of nulltons as NM rounds. Specifically, let  $\mathcal{L}$  with  $|\mathcal{L}| = \bar{L}$  denote the set of NM rounds. We can utilize the robust scheme developed in Section IV.C to estimate the location of the largest entry in  $\mathbf{\Lambda}$ , i.e.,

$$(i^*, j^*) = \max_{(i,j) \in \mathcal{F}} \prod_{l \in \mathcal{L}} \mathcal{P}^{(l)}(i, j) \quad (55)$$

where  $\mathcal{P}^{(l)}(i, j)$  is defined in (43).

For clarity, the algorithm is summarized in Algorithm 2. Following a similar analysis in Section IV.C, we know that the proposed scheme has a computational complexity of order  $\mathcal{O}(MN_t \bar{L})$ , where  $\bar{L}$  denotes the number of NM rounds.

---

#### Algorithm 2 Proposed beam alignment algorithm for NLOS scenarios

---

- 1: Generate  $\{\mathbf{A}_l\}_{l=1}^L$  according to Section III.A;
  - 2: Generate  $\{\mathbf{C}_l\}_{l=1}^L$  according to Section III.B;
  - 3: Obtain received signals  $\{\mathbf{Y}_l\}_{l=1}^L$  for  $L$  rounds;
  - 4: **for**  $l = 1, \dots, L$  **do**
  - 5: Determine whether the received signal  $Y_l(u_l, v_l)$  is a nullton or not via the energy detector (54). Count the number of nulltons for each round.
  - 6: **end for**
  - 7: Find rounds with the smallest number of nulltons and regard them as NM rounds.
  - 8: **for**  $l = 1, \dots, L$  **do**
  - 9: **if** the round- $l$  is an NM round **then**
  - 10: Calculate the ‘‘probability’’ function via (43) for all indices  $(i, j)$ .
  - 11: **end if**
  - 12: **end for**
  - 13: Determine the best beam direction index  $(i^*, j^*)$  of the dominant element in  $\mathbf{\Lambda}$  via (55).
-

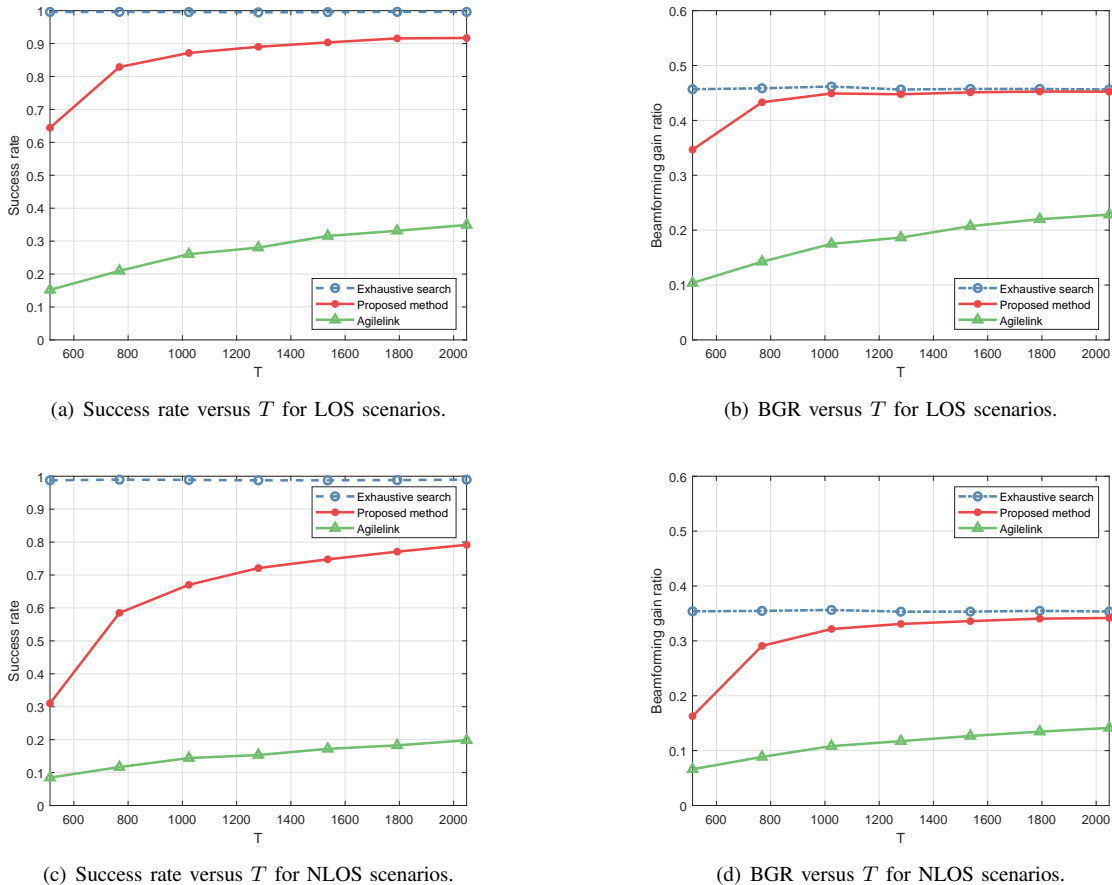


Fig. 4. Success rate and beamforming gain ratio versus  $T$  for LOS and NLOS scenarios in the noisy case,  $\text{SNR} = -20\text{dB}$ .

## VI. SIMULATION RESULTS

In this section, we provide simulation results to illustrate the performance of our proposed method. In our simulations, we consider a mmWave system operating at a carrier frequency of 28GHz. For the large-scale path loss, the reference channel power gain at a distance of 1m is set as  $g_0 = -61.3\text{dB}$ , the path loss exponents of the BS-IRS and IRS-user links are set as  $\gamma_{BI} = 2.3$  and  $\gamma_{IU} = 2$  respectively [28]. The small-scale fading is modeled by Rician fading, with the BS-IRS Rician factors set as 13.2dB and the IRS-user Rician factors set as 13.2dB for LOS scenarios and 0dB for NLOS scenarios. Also, we assume the IRS adopts a UPA with  $M = M_y \times M_z = 16 \times 16 = 256$  elements, and the BS employs a ULA with  $N_t = 128$  antennas. Two metrics are used to evaluate the performance of the proposed method, namely, the success rate which is computed as the ratio of finding the correct index of the largest (in magnitude) component in  $\Lambda$ , and the beamforming gain ratio (BGR) which is defined as

$$\gamma_{\text{bf}} \triangleq \mathbb{E} \left[ \frac{\|\mathbf{v}^H \mathbf{H} \mathbf{f}\|^2}{\|\mathbf{v}_{\text{opt}}^H \mathbf{H} \mathbf{f}_{\text{opt}}\|^2} \right] \quad (56)$$

where  $\mathbf{v}_{\text{opt}}$  and  $\mathbf{f}_{\text{opt}}$  are optimally devised by assuming the full knowledge of the cascade channel  $\mathbf{H}$  via the method developed in [7],  $\mathbf{v}$  and  $\mathbf{f}$  are devised to align the BS's and IRS's beams to the strongest path, i.e.,  $\mathbf{v} = \sqrt{M} \mathbf{D}_R(:, i^*)$ ,

$\mathbf{f} = \mathbf{D}_{N_t}(:, j^*)$ , and  $(i^*, j^*)$  denotes the estimated index of the largest component in  $\Lambda$ . For a fair comparison, the transmit beamforming vectors  $\mathbf{f}(t)$  used by our proposed method and other competing beam alignment schemes are normalized to unit norm throughout our simulations. The signal-to-noise ratio (SNR) is defined as  $10 \log_{10}(\|\mathbf{H}\|_F^2 / (N_t M \sigma^2))$ .

We now examine the performance of our proposed method and compare it with the exhaustive beam search scheme discussed in Section II.C and the state-of-the-art AgileLink scheme [24]. AgileLink is a beam alignment scheme which also relies on the magnitude of measurements for recovery of signal directions. Although originally developed for conventional mmWave systems, its variant for array transmitter and receiver (see Section 4.4 of [24]) can be readily applied to IRS-assisted mmWave systems since the IRS-assisted signal model can be thought of as a conventional MIMO model. AgileLink divides both the BS antennas and IRS elements into several subarrays to form hashing beam patterns. For our proposed method, the sparse encoding matrices  $\{\mathbf{C}_I\}$  are generated via the optimization-based method (29) such that the corresponding passive beamforming vectors are of constant modulus. In our simulations, we set  $P = 2$ ,  $P' = 2$ , and the AoAs and AoDs are randomly generated without assuming lying on the discretized grid. For the LOS scenario, we assume that the Rician factors for both the BS-IRS channel (4) and the IRS-user channel (10) are set to 13.2dB [32], [40]. For the

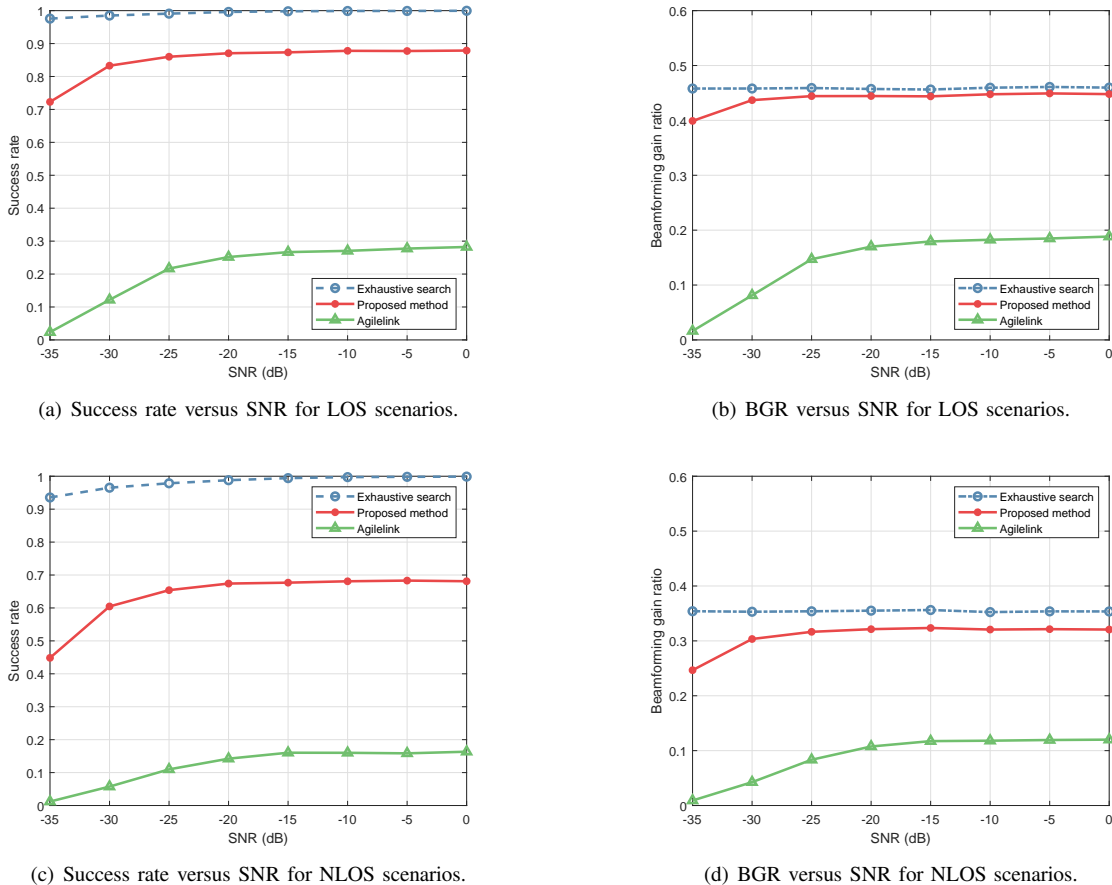


Fig. 5. Success rate and beamforming gain ratio versus SNR for LOS and NLOS scenarios in the noisy case,  $T = 1024$ .

NLOS scenario, the Rician factor for the IRS-user channel is set to 0dB to simulate the scenario where there are multiple comparable paths from the IRS to the user.

In Fig. 4, we plot the success rates and beamforming gain ratios of respective methods as a function of the total number of measurements  $T$ , where the SNR is set to  $\text{SNR} = -20\text{dB}$ . For our proposed method, we set  $R = 8$  and  $Q = 16$  and vary  $L$  from 2 to 8, while for the AgileLink, for each value of  $T$ , its parameters are carefully adjusted to achieve its best performance. The exhaustive search scheme is included to provide the best achievable performance for any beam alignment schemes, but it requires as many as  $T = MN_t = 32768$  measurements in total. From Fig. 4, it can be seen that the proposed method achieves a significant performance improvement over the AgileLink scheme for both the LOS and NLOS scenarios. Also, we observe that our proposed method, with only a mild number of measurements (say,  $T = 1792$ ), can achieve a beamforming gain close to the exhaustive search scheme. Specifically, to achieve performance similar to the exhaustive search scheme, the training overhead required by our proposed method is only about 5% of that needed by the exhaustive search scheme.

In Fig. 5, we plot the success rates and beamforming gain ratios of respective methods as a function of the SNR, where the number of measurements is set to  $T = UVL = 16 \times 16 \times 4 = 1024$ . From Fig. 5, we can see that our proposed

method performs well even when the SNR is as low as  $-35\text{dB}$ . Also, the performance of our proposed method is close to that of the exhaustive search scheme while the proposed method requires only 1024 measurements, thus enjoying a substantial training overhead reduction compared to the exhaustive search scheme of  $T = MN_t = 32768$ . Moreover, the proposed method outperforms the AgileLink scheme by a big margin across different SNR regimes.

To examine the impact of the number of reflecting elements on the proposed beam training method, in Fig. 6, we plot the success rates and beamforming gain ratios of respective algorithms versus the number of reflecting elements for LOS scenarios, where the SNR is set to  $-20\text{dB}$  and the total number of measurements used for training (except the exhaustive search scheme) is set to  $T = 1024$ . For our proposed method, we set  $U = 16$ ,  $V = 16$ , and  $L = 4$ . Note that to make  $U = M/Q$  unchanged, we adjust the value of  $Q$  accordingly for different choices of  $M$ . It can be observed that the success rate of the proposed method keeps almost unaltered as the number of reflecting elements  $M$  increases, whereas the AgileLink incurs a certain amount of performance loss as  $M$  grows.

Finally, to compare with SwiftLink, a fast compressed sensing-based beam alignment algorithm that is robust against the CFO [18], we consider a simplified scenario where the BS has the knowledge of the location of the IRS and has aligned its beam to the LOS component between the BS and

the IRS. In this case, we only need to focus on beam training between the IRS and the user. Our proposed method can be readily applied to this scenario. Unlike AgileLink, SwiftLink cannot be straightforwardly extended to joint BS-IRS-user beam training. But it can be directly applied to this simplified scenario by treating the IRS as an active transmitter. In our simulations, we set CFO = 20ppm, the carrier frequency is set to 28GHz, the bandwidth is set to 30MHz and the phase noise is set to zero. Also, due to the limitation inherent in the trajectory design, SwiftLink only allows a limited number of measurements for training, i.e.  $T \in \{T \leq 4M_y - 2, \text{ and } T = 4x, x \text{ is an integer}\}$ . To satisfy this condition, we set  $T = 60$  for SwiftLink. For a fair comparison, the number of measurements for Agilelink and our proposed method is set to  $T = 64$ . Fig. 7 depicts success rates and beamforming gain ratios of respective algorithms. It can be observed that our proposed method presents a substantial performance improvement over Swiftlink, particularly in the low SNR regime. Since SwiftLink comprises several sequential stages, the estimation accuracy of both the CFO and the channel depends on the estimation results obtained in the previous stages. Also, it is known that compressed sensing algorithms tend to be fragile in low-SNR scenarios. In contrast, our proposed method uses multi-directional beams to probe the channel and relies on prominent measurements to identify the beam directions, and thus is more resilient to low SNRs. This is probably the reason why our proposed method outperforms SwiftLink, particularly in the low SNR regime.

## VII. CONCLUSIONS

In this paper, we studied the problem of beam alignment for IRS-assisted mmWave/THz downlink systems. By exploiting the inherent sparse structure of the BS-IRS-user cascade channel, we devised multi-directional beam training sequences to scan the angular space and proposed an efficient set-intersection-based scheme to identify the best beam alignment from compressive phaseless measurements. Theoretical and numerical results show that the proposed method can perform reliable beam alignment in the low SNR regime with a substantially reduced beam training overhead.

### APPENDIX A PROOF OF THEOREM 1

We first define

$$\mathcal{S} \triangleq \left\{ (i, j) \mid i \in \bigcap_{l=1}^L \mathcal{S}_{u_l}^{(l)}, j \in \bigcap_{l=1}^L \mathcal{S}_{v_l}^{(l)} \right\} \quad (57)$$

From (32), we have  $(i^*, j^*) \in \mathcal{S}$ . Let  $B_x \triangleq \{|\mathcal{S}| = x\}$  denote the event that the set  $\mathcal{S}$  contains  $RQ \geq x \geq 1$  elements in total, and  $Z$  denote the event of identifying the location of the largest element in  $\lambda$ . We therefore have

$$\Pr(Z) = \sum_{x=1}^{RQ} \Pr(Z|B_x) \Pr(B_x) \quad (58)$$

where

$$\Pr(Z|B_x) = \frac{1}{x} \quad (59)$$

Clearly, we have  $\Pr(Z) \geq \Pr(B_1)$ . For simplicity, we only analyze the probability that the intersection set  $\mathcal{S}$  contains only one element.

Let  $\mathcal{C}_l \triangleq \mathcal{S}_{u_l}^{(l)} - \{i^*\}$  and  $\mathcal{A}_l \triangleq \mathcal{S}_{v_l}^{(l)} - \{j^*\}$ . Define  $\mathcal{S}_c \triangleq \bigcap_{l=1}^L \mathcal{C}_l$  as the intersection set of the row indices, and  $\mathcal{S}_a \triangleq \bigcap_{l=1}^L \mathcal{A}_l$  as the intersection set of column indices. Then we have

$$\Pr(B_1) = \Pr(\mathcal{S}_c = \emptyset) \times \Pr(\mathcal{S}_a = \emptyset) \quad (60)$$

Since the two events  $\mathcal{S}_c = \emptyset$  and  $\mathcal{S}_a = \emptyset$  are mutually independent, we can first calculate  $\Pr(\mathcal{S}_c = \emptyset)$  and the latter can be obtained similarly.

Note that

$$\Pr(\mathcal{S}_c = \emptyset) = 1 - \Pr(\mathcal{S}_c \neq \emptyset) \quad (61)$$

we now derive the probability of the event that the intersection set  $\mathcal{S}_c$  is non-empty. Without loss of generality, we assume  $i^* = M$ . Let  $D_m$  denote the event of  $m \in \mathcal{S}_c$ . It can be easily verified that

$$\Pr\left(\bigcap_{m \in J} D_m\right) = \left(\frac{\binom{M-1-j}}{\binom{M-1}}\right)^L, \quad J \subset \{1, 2, \dots, M-1\}, |J| = j, j = 1, \dots, Q-1 \quad (62)$$

The probability of the set  $\mathcal{S}_c$  being non-empty can be calculated as

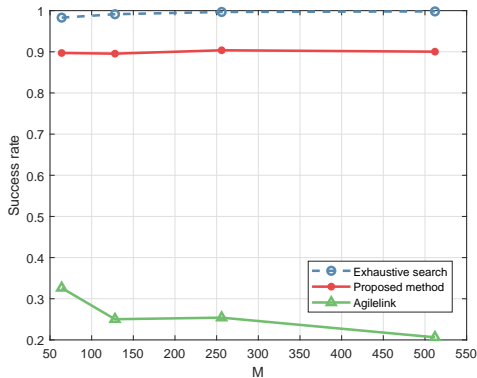
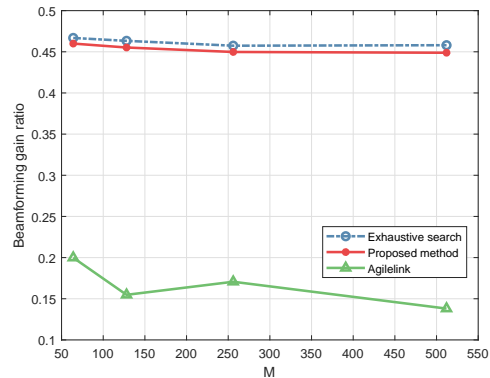
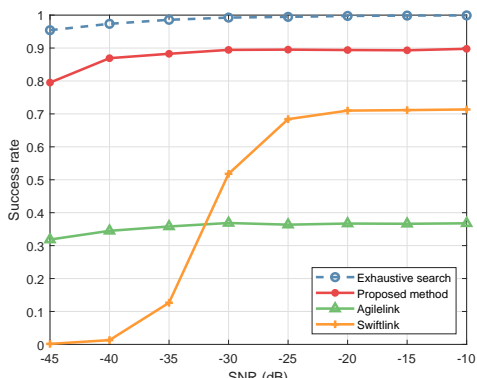
$$\begin{aligned} \Pr(\mathcal{S}_c \neq \emptyset) &= \Pr\left(\bigcup_{m=1}^{M-1} D_m\right) \\ &\stackrel{(a)}{=} \sum_{j=1}^{M-1} (-1)^{j-1} \sum_{J \subset \{1, 2, \dots, M-1\}, |J|=j} \Pr\left(\bigcap_{m \in J} D_m\right) \\ &\stackrel{(b)}{=} \sum_{j=1}^{Q-1} (-1)^{j-1} \sum_{J \subset \{1, 2, \dots, M-1\}, |J|=j} \Pr\left(\bigcap_{m \in J} D_m\right) \\ &\stackrel{(c)}{=} \sum_{j=1}^{Q-1} (-1)^{(j-1)} \binom{M-1}{j} \left(\frac{\binom{M-1-j}}{\binom{M-1}}\right)^L \\ &\stackrel{(d)}{\leq} (M-1) \left(\frac{Q-1}{M-1}\right)^L \end{aligned} \quad (63)$$

where (a) follows from the principle of inclusion-exclusion, in (b), we utilize the property that

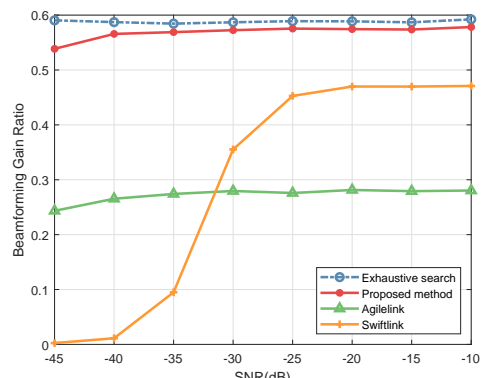
$$\Pr\left(\bigcap_{m \in J} D_m\right) = 0, \quad \forall |J| \geq Q \quad (64)$$

since the intersection set  $\mathcal{S}_c$  contains at most  $Q-1$  elements, (c) comes from the fact that there are  $\binom{M-1}{j}$  ways to select  $j$  elements from the set  $\{1, 2, \dots, M-1\}$  to make  $|J| = j$ , and (d) follows from

$$\Pr\left(\bigcup_{m=1}^{M-1} D_m\right) \leq \sum_{m=1}^{M-1} \Pr(D_m) = (M-1) \Pr(D_m) \quad (65)$$

(a) Success rate versus  $M$  for LOS scenarios(b) BGR versus  $M$  for LOS scenarios.Fig. 6. Success rate and beamforming gain ratio versus the number of reflecting elements  $M$  for LOS scenarios.

(a) Success rate versus SNR for LOS scenarios



(b) BGR versus SNR for LOS scenarios.

Fig. 7. Success rate and beamforming gain ratio versus SNR for LOS scenarios when the BS-IRS channel is perfectly aligned.

As a result, we have

$$\begin{aligned} \Pr(\mathcal{S}_c = \emptyset) &= 1 - \Pr(\mathcal{S}_c \neq \emptyset) \\ &\stackrel{(a)}{\geq} 1 - (M-1) \left( \frac{Q-1}{M-1} \right)^L \\ &= P(Q, L, M) \end{aligned} \quad (66)$$

where (a) is derived from (63).

Similarly, we have

$$\Pr(\mathcal{S}_a = \emptyset) \geq 1 - (N_t - 1) \left( \frac{R-1}{N_t-1} \right)^L = P(R, L, N_t) \quad (67)$$

Therefore the probability of identifying the location of the largest component in  $\mathbf{\Lambda}$  is no smaller than

$$P = \Pr(Z) \geq P(Q, L, M) \times P(R, L, N_t) \quad (68)$$

This completes our proof.

#### APPENDIX B PROOF OF THEOREM 2

Let  $X$  denote the number of NM rounds out of the total  $L$  full-coverage rounds of scanning, and  $\tilde{Z}$  denote the event

of exact recovery of the location of the largest element. Specifically, define a random variable

$$X_l \triangleq \begin{cases} 1, & \text{if round } l \text{ is a NM round} \\ 0, & \text{if round } l \text{ is not a NM round} \end{cases} \quad (69)$$

Thus  $X$  can be expressed as

$$X \triangleq \sum_{l=1}^L X_l. \quad (70)$$

Clearly, the random variables  $\{X_l\}$  are mutually independent and identically distributed with  $\Pr(X_l = 1) = p$ ,  $\Pr(X_l = 0) = 1 - p$ . The random variable  $X$ , therefore, follows a binomial distribution, i.e.,  $X \sim \mathcal{B}(L, p)$ . Thus we have

$$\begin{aligned} \Pr(\tilde{Z}) &= \sum_{l=0}^L \Pr(\tilde{Z}|X=l) \Pr(X=l) \\ &\stackrel{(a)}{=} \sum_{l=0}^L \Pr(\tilde{Z}|X=l) \binom{L}{l} p^l (1-p)^{L-l} \\ &\stackrel{(b)}{\geq} \sum_{l=0}^L g(Q, l, M) \times g(R, l, N_t) \times \left( \binom{L}{l} p^l (1-p)^{L-l} \right) \end{aligned} \quad (71)$$

where (a) is obtained from the probability mass function of the binomial distribution; and in (b), we directly apply the equality (c) of (63).

## REFERENCES

- [1] J. Zhang, E. Björnson, M. Matthaiou, D. W. K. Ng, H. Yang, and D. J. Love, "Prospective multiple antenna technologies for beyond 5G," *IEEE J. Sel. Areas Commun.*, vol. 38, no. 8, pp. 1637–1660, Aug. 2020.
- [2] X. Tan, Z. Sun, D. Koutsonikolas, and J. M. Jornet, "Enabling indoor mobile millimeter-wave networks based on smart reflect-arrays," in *Proc. IEEE Int. Conf. Comput. Commun. (INFOCOM)*, Honolulu, Hawaii, Apr. 15–19 2018, pp. 270–278.
- [3] P. Wang, J. Fang, X. Yuan, Z. Chen, H. Duan, and H. Li, "Intelligent reflecting surface-assisted millimeter wave communications: Joint active and passive precoding design," *IEEE Trans. Veh. Technol.*, vol. 69, no. 12, pp. 14960–14973, Dec. 2020.
- [4] N. S. Perović, M. Di Renzo, and M. F. Flanagan, "Channel capacity optimization using reconfigurable intelligent surfaces in indoor mmwave environments," in *Proc. IEEE Int. Conf. Commun. (ICC)*, Jun. 7–11 2020, pp. 1–7.
- [5] Q. Wu and R. Zhang, "Intelligent reflecting surface enhanced wireless network via joint active and passive beamforming," *IEEE Trans. Wireless Commun.*, vol. 18, no. 11, pp. 5394–5409, Nov. 2019.
- [6] P. Wang, J. Fang, L. Dai, and H. Li, "Joint transceiver and large intelligent surface design for massive MIMO mmwave systems," *IEEE Trans. Wireless Commun.*, vol. 20, no. 2, pp. 1052–1064, Feb. 2021.
- [7] X. Yu, D. Xu, and R. Schober, "MISO wireless communication systems via intelligent reflecting surfaces," in *Proc. IEEE/CIC Int. Conf. Commun. China (ICCC)*, Aug. 2019, pp. 735–740.
- [8] B. Ning, Z. Chen, W. Chen, and J. Fang, "Beamforming optimization for intelligent reflecting surface assisted MIMO: A sum-path-gain maximization approach," *IEEE Wireless Commun. Lett.*, vol. 9, no. 7, pp. 1105–1109, Jul. 2020.
- [9] S. Zhang and R. Zhang, "Capacity characterization for intelligent reflecting surface aided MIMO communication," *IEEE J. Sel. Areas Commun.*, vol. 38, no. 8, pp. 1823–1838, Aug. 2020.
- [10] D. Mishra and H. Johansson, "Channel estimation and low-complexity beamforming design for passive intelligent surface assisted MISO wireless energy transfer," in *Proc. IEEE Int. Conf. Acoust. Speech Signal Process. (ICASSP)*, Brighton, UK, May 12–17 2019, pp. 4659–4663.
- [11] T. L. Jensen and E. De Carvalho, "An optimal channel estimation scheme for intelligent reflecting surfaces based on a minimum variance unbiased estimator," in *Proc. IEEE Int. Conf. Acoust., Speech Signal Process. (ICASSP)*, May, 2020, pp. 5000–5004.
- [12] X. Guan, Q. Wu, and R. Zhang, "Anchor-assisted channel estimation for intelligent reflecting surface aided multiuser communication," *IEEE Trans. Wireless Commun.*, 2021, [Online]. Available: <https://arxiv.org/abs/2102.10886>.
- [13] P. Wang, J. Fang, H. Duan, and H. Li, "Compressed channel estimation and joint beamforming for intelligent reflecting surface-assisted millimeter wave systems," *IEEE Signal Process. Lett.*, vol. 27, pp. 905–909, May 2020.
- [14] J. Chen, Y.-C. Liang, H. V. Cheng, and W. Yu, "Channel estimation for reconfigurable intelligent surface aided multi-user MIMO systems," 2019 [Online]. Available: <https://arxiv.org/abs/1912.03619>.
- [15] Z.-Q. He and X. Yuan, "Cascaded channel estimation for large intelligent metasurface assisted massive MIMO," *IEEE Wireless Commun. Lett.*, vol. 9, no. 2, pp. 210–214, Feb. 2019.
- [16] S. Liu, Z. Gao, J. Zhang, M. Di Renzo, and M.-S. Alouini, "Deep denoising neural network assisted compressive channel estimation for mmwave intelligent reflecting surfaces," *IEEE Trans. Veh. Technol.*, vol. 69, no. 8, pp. 9223–9228, Aug. 2020.
- [17] N. J. Myers and R. W. Heath, "A compressive channel estimation technique robust to synchronization impairments," in *2017 IEEE 18th Int. Workshop Signal Process. Advances Wireless Commun. (SPAWC)*. IEEE, Jul. 2017, pp. 1–5.
- [18] N. J. Myers, A. Mezghani, and R. W. Heath, "Swift-link: A compressive beam alignment algorithm for practical mmwave radios," *IEEE Trans. Signal Process.*, vol. 67, no. 4, pp. 1104–1119, Feb. 2019.
- [19] N. J. Myers and R. W. Heath, "Message passing-based joint CFO and channel estimation in mmwave systems with one-bit ADCs," *IEEE Trans. Wireless Commun.*, vol. 18, no. 6, pp. 3064–3077, Jun. 2019.
- [20] T. Van Chien, H. Q. Ngo, S. Chatzinotas, M. Di Renzo, and B. Ottersten, "Reconfigurable intelligent surface-assisted cell-free massive MIMO systems over spatially-correlated channels," Apr. 2021, [Online]. Available: <https://arxiv.org/abs/2104.08648>.
- [21] A. Alkhateeb, O. El Ayach, G. Leus, and R. W. Heath, "Channel estimation and hybrid precoding for millimeter wave cellular systems," *IEEE J. Sel. Topics Signal Process.*, vol. 8, no. 5, pp. 831–846, Oct. 2014.
- [22] Z. Xiao, T. He, P. Xia, and X.-G. Xia, "Hierarchical codebook design for beamforming training in millimeter-wave communication," *IEEE Trans. Wireless Commun.*, vol. 15, no. 5, pp. 3380–3392, May. 2016.
- [23] S. Noh, M. D. Zoltowski, and D. J. Love, "Multi-resolution codebook and adaptive beamforming sequence design for millimeter wave beam alignment," *IEEE Trans. Wireless Commun.*, vol. 16, no. 9, pp. 5689–5701, Sept. 2017.
- [24] H. Hassanieh, O. Abari, M. Rodriguez, M. Abdelghany, D. Katabi, and P. Indyk, "Fast millimeter wave beam alignment," in *Proc. ACM Spec. Interest Group Data Commun.*, Budapest, Hungary, Aug. 2018, pp. 432–445.
- [25] W. Wu, N. Cheng, N. Zhang, P. Yang, W. Zhuang, and X. Shen, "Fast mmwave beam alignment via correlated bandit learning," *IEEE Trans. Wireless Commun.*, vol. 18, no. 12, pp. 5894–5908, Dec. 2019.
- [26] X. Li, J. Fang, H. Duan, Z. Chen, and H. Li, "Fast beam alignment for millimeter wave communications: A sparse encoding and phaseless decoding approach," *IEEE Trans. Signal Process.*, vol. 67, no. 17, pp. 4402–4417, Sept. 2019.
- [27] B. Ning, Z. Chen, W. Chen, Y. Du, and J. Fang, "Terahertz multi-user massive MIMO with intelligent reflecting surface: Beam training and hybrid beamforming," *IEEE Trans. Veh. Technol.*, vol. 70, no. 2, pp. 1376–1393, Feb. 2021.
- [28] C. You, B. Zheng, and R. Zhang, "Fast beam training for IRS-assisted multiuser communications," *IEEE Wireless. Commun. Lett.*, vol. 9, no. 11, pp. 1845–1849, Nov. 2020.
- [29] W. Wang and W. Zhang, "Joint beam training and positioning for intelligent reflecting surfaces assisted millimeter wave communications," *IEEE Trans. Wireless Commun.*, 2021.
- [30] X. Hu, C. Zhong, Y. Zhu, X. Chen, and Z. Zhang, "Programmable metasurface-based multicast systems: Design and analysis," *IEEE J. Sel. Areas Commun.*, vol. 38, no. 8, pp. 1763–1776, Aug. 2020.
- [31] H. Wang, J. Fang, P. Wang, G. Yue, and H. Li, "Efficient beamforming training and channel estimation for millimeter wave OFDM systems," *IEEE Trans. Wireless Commun.*, vol. 20, no. 5, pp. 2805–2819, May 2021.
- [32] O. E. Ayach, S. Rajagopal, S. Abu-Surra, Z. Pi, and R. W. Heath, "Spatially sparse precoding in millimeter wave MIMO systems," *IEEE Trans. Wireless Commun.*, vol. 13, no. 3, pp. 1499–1513, Mar. 2014.
- [33] T. Jiang, J. Zhang, M. Shafi, L. Tian, and P. Tang, "The comparative study of S-V model between 3.5 and 28 GHz in indoor and outdoor scenarios," *IEEE Trans. Veh. Technol.*, vol. 69, no. 3, pp. 2351–2364, Mar. 2020.
- [34] C. Han, A. O. Bicen, and I. F. Akyildiz, "Multi-ray channel modeling and wideband characterization for wireless communications in the terahertz band," *IEEE Trans. Wireless Commun.*, vol. 14, no. 5, pp. 2402–2412, May 2015.
- [35] C. Lin and G. Y. Li, "Indoor terahertz communications: How many antenna arrays are needed?" *IEEE Trans. Wireless Commun.*, vol. 14, no. 6, pp. 3097–3107, Jun. 2015.
- [36] C. Han, J. M. Jornet, and I. Akyildiz, "Ultra-massive MIMO channel modeling for graphene-enabled terahertz-band communications," in *2018 IEEE 87th Veh. Technol. Conf. (VTC Spring)*, 3–6, Jun. 2018, pp. 1–5.
- [37] H. Tataria, M. Shafi, A. F. Molisch, M. Dohler, H. Sjöland, and F. Tufvesson, "6G wireless systems: Vision, requirements, challenges, insights, and opportunities," *Proc. IEEE*, vol. 109, no. 7, pp. 1166–1199, Jul. 2021.
- [38] S. Abeywickrama, R. Zhang, Q. Wu, and C. Yuen, "Intelligent reflecting surface: Practical phase shift model and beamforming optimization," *IEEE Trans. Commun.*, vol. 68, no. 9, pp. 5849–5863, Sept. 2020.
- [39] W. Tang, M. Z. Chen, X. Chen, J. Y. Dai, Y. Han, M. Di Renzo, Y. Zeng, S. Jin, Q. Cheng, and T. J. Cui, "Wireless communications with reconfigurable intelligent surface: Path loss modeling and experimental measurement," *IEEE Trans. Wireless Commun.*, vol. 20, no. 1, pp. 421–439, Jan. 2021.
- [40] M. R. Akdeniz, Y. Liu, M. K. Samimi, S. Sun, S. Rangan, T. S. Rappaport, and E. Erkip, "Millimeter wave channel modeling and cellular capacity evaluation," *IEEE J. Sel. Areas Commun.*, vol. 32, no. 6, pp. 1164–1179, Jun. 2014.

- [41] Z. Muhi-Eldeen, L. Ivrisimtzis, and M. Al-Nuaimi, "Modelling and measurements of millimetre wavelength propagation in urban environments," *IET Microw. Antennas & Propag.*, vol. 4, no. 9, pp. 1300–1309, Sept. 2010.
- [42] S. Priebe, M. Kannicht, M. Jacob, and T. Kürner, "Ultra broadband indoor channel measurements and calibrated ray tracing propagation modeling at THz frequencies," *J. Commun. Netw.*, vol. 15, no. 6, pp. 547–558, Dec. 2013.